Field-enhancing photonic devices utilizing waveguide coupling and plasmonics - a selection rule for optimization-based design

Vester-Petersen, Joakim; Madsen, Søren P.; Sigmund, Ole; Balling, Peter; Julsgaard, Brian ; Christiansen, Rasmus Ellebæk

Published in:
Optics Express

Link to article, DOI:
10.1364/OE.26.00A788

Publication date:
2018

Document Version
Publisher's PDF, also known as Version of record

Research Article | Vol. 26, No. 18 | 3 Sep 2018 | OPTICS EXPRESS A788
Optics EXPRESS

Field-enhancing photonic devices utilizing waveguide coupling and plasmonics - a selection rule for optimization-based design

JOAKIM VESTER-PETERSEN,[1,*] SØREN P. MADSEN,[1] OLE SIGMUND,[2] PETER BALLING,[3,4] BRIAN JULSGAARD,[3,4] AND RASMUS E. CHRISTIANSEN[2]

[1]*Department of Engineering, Aarhus University, Inge Lehmanns Gade 10, 8000 Aarhus C, Denmark*
[2]*Department of Mechanical Engineering, Technical University of Denmark, Nils Koppels Alle, Building 404, 2800 Kgs. Lyngby, Denmark*
[3]*Department of Physics and Astronomy, Aarhus University, Ny Munkegade 120, 8000 Aarhus C, Denmark*
[4]*Interdisciplinary Nanoscience Center (iNANO), Aarhus University, Gustav Wieds Vej 14, 8000 Aarhus C, Denmark*
[*]*jvepe@eng.au.dk*

Abstract: This paper describes a systematic design study of periodic gold-nanostrip arrays placed on a thin film aimed at enhancing the electric field inside the film when irradiated by light. Based on the study, a "selection rule" is proposed, which provides optimization-based design methods with an a priori choice between field-enhancement dominated by coupling to guided modes, by plasmonic near-field enhancement or by a mix hereof. An appropriate choice of wavelength and grating period is shown to selectively suppress or include waveguiding effects for the optimized designs. The validity of the selection rule is demonstrated through a numerical topology optimization study in which gold nanostrips are optimized for electric-field enhancement in an erbium-doped TiO_2 thin film, targeting increased spectral upconversion in the erbium ions. The obtained designs exhibit waveguide excitation within the predicted intervals and, for light polarized perpendicularly to the strips, plasmonic response outside.

OCIS codes: (050.0050) Diffraction and gratings; (190.7220) Upconversion; (230.0230) Optical devices; (230.74009) Waveguides, slab; (250.5403) Plasmonics.

References and links

1. H. G. Frey, F. Keilmann, A. Kriele, and R. Guckenberger, "Enhancing the resolution of scanning near-field optical microscopy by a metal tip grown on an aperture probe,", Appl. Phys. Lett. **81**, 5030 (2002).
2. M. Mansuripur, A. R. Zakharian, A. Lesuffleur, S.-H. Oh, R. J. Jones, N. C. Lindquist, H. Im, A. Kobyakov, and J. V. Moloney, "Plasmonic nano-structures for optical data storage," Opt. Express **17**, 14001–14014 (2009).
3. S. R. Johannsen, S. P. Madsen, B. R. Jeppesen, J. V. Nygaard, B. Julsgaard, P. Balling, and A. N. Larsen, "Up-conversion enhancement in Er^{3+} doped TiO_2 through plasmonic coupling: Experiments and finite-element modeling," Appl. Phys. Lett. **106**, 053101 (2015).
4. H. Lakhotiya, A. Nazir, S. P. Madsen, J. Christiansen, E. Eriksen, J. Vester-Petersen, S. R. Johannsen, B. R. Jeppesen, P. Balling, A. N. Larsen, and B. Julsgaard, "Plasmonically enhanced upconversion of 1500 nm light via trivalent Er in a TiO2 matrix," Appl. Phys. Lett. **109**, 263102 (2016).
5. E. Wadbro, and C. Engström, "Topology and shape optimization of plasmonic nano-antennas," Comput. Methods Appl. Mech. Eng. **293**, 155–169 (2015).
6. J. Vester-Petersen, R. E. Christiansen, B. Julsgaard, P. Balling, O. Sigmund, and S. P. Madsen, "Topology optimized gold nanostrips for enhanced near-infrared photon upconversion," Appl. Phys. Lett. **111**, 133102 (2017).
7. R. E. Christiansen, J. Vester-Petersen, O. Sigmund, and S. P. Madsen, "A non-linear material interpolation for design of metallic nano-particles using topology optimization," Submitted (2018).
8. J. C. Goldschmidt and S. Fischer, "Upconversion for photovoltaics - a review of materials, devices and concepts for performance enhancement," Adv. Opt. Mater. **3**, 510–535 (2015).
9. K. Ogawa, W. Chang, B. Sopori, and F. Rosenbaum, "A theoretical analysis of etched grating couplers for integrated optics," IEEE J. Quantum Electron. **9**, 29–42 (1973).
10. T. Tamir and S. T. Peng, "Analysis and design of grating couplers," Appl. Phys. **14**, 235–254 (1977).

#330789 https://doi.org/10.1364/OE.26.00A788
Journal © 2018 Received 14 May 2018; revised 10 Jul 2018; accepted 10 Jul 2018; published 24 Jul 2018

Optics EXPRESS

11. S. Nie, "Probing Single Molecules and Single Nanoparticles by Surface-Enhanced Raman Scattering," Science **275**, 1102–1106 (1997).
12. D. Threm, Y. Nazirizadeh, and M. Gerken, "Photonic crystal biosensors towards on-chip integration," J. Biophotonics **5**, 601–616 (2012).
13. I. Koirala, V. R. Shrestha, C.-S. Park, S.-S. Lee, and D.-Y. Choi, "Polarization-Controlled Broad Color Palette Based on an Ultrathin One-Dimensional Resonant Grating Structure," Sci. Rep. **7**, 40073 (2017).
14. J.-M. Jin, *The Finite Element Method in Electromagnetics*, 3rd ed. (Wiley-IEEE, 2014).
15. COMSOL AB, "COMSOL Multiphysics® v. 5.3".
16. A. Yariv and P. Yeh, *Photonics* (Oxford University, 2006).
17. R. D. Kekatpure, A. C. Hryciw, E. S. Barnard, and M. L. Brongersma, "Solving dielectric and plasmonic waveguide dispersion relations on a pocket calculator," Opt. Express **17**, 24112–24129 (2009).
18. M. Pollnau, D. R. Gamelin, S. R. Lüthi, H. U. Güdel, and M. P. Hehlen, "Power dependence of upconversion luminescence in lanthanide and transition-metal-ion systems," Phys. Rev. B **61**, 3337–3346 (2000).
19. M. P. Bendsøe and O. Sigmund, *Topology Optimization* (Springer, 2004).
20. J. Jensen and O. Sigmund, "Topology optimization for nano-photonics", Laser & Photonics Rev. **5**, 308–321 (2011).
21. S. P. Madsen, S. R. Johannsen, B. R. Jeppesen, J. V. Nygaard, P. B. Jensen, J. Chevallier, B. Julsgaard, P. Balling, and A. N. Larsen, "Optimizing Plasmonically Enhanced Upconversion," Energy Procedia **77**, 478–486 (2015).
22. A. D. Rakić, A. B. Djurišić, J. M. Elazar, and M. L. Majewski, "Optical properties of metallic films for vertical-cavity optoelectronic devices," Appl. Opt. **37**, 5271–5283 (1998).
23. I. H. Malitson, "Interspecimen Comparison of the Refractive Index of Fused Silica," J. Opt. Soc. Am. **55**, 1205–1209 (1965).
24. K. Svanberg, "MMA and GCMMA - two methods for nonlinear optimization," 1–15 (2007).
25. J. J. Mock, M. Barbic, D. R. Smith, D. A. Schultz, and S. Schultz, "Shape effects in plasmon resonance of individual colloidal silver nanoparticles," J. Chem. Phys. **116**, 6755–6759 (2002).
26. O. Sigmund, "Manufacturing tolerant topology optimization," Acta Mech. Sinica **25**, 227–239 (2009).
27. R. E. Christiansen, B. S. Lazarov, J. S. Jensen, and O. Sigmund, "Creating geometrically robust designs for highly sensitive problems using topology optimization: Acoustic cavity design," Struct. Multidiscip. Optim. **52**, 737–754 (2015).

1. Introduction

Localized enhancement of the electric field under external irradiation is desirable for a range of applications. Examples include, near-field optical microscopy [1], optically assisted data storage [2], and enhanced ionic luminescence [3, 4]. Obtaining high enhancement factors is possible through careful optimization of the system under design [5–7]. The application, considered in the following is enhanced spectral upconversion of sunlight, which is a promising way of improving the limited absorption in photovoltaic devices [8]. Spectral upconversion relies on an optically active medium (e.g. erbium ions) to convert low-energy photons below the band gap of the absorber into photons of higher energy within the absorption band, thereby contributing to the current production. For efficient upconversion it is, however, necessary to concentrate the electric field in local areas of the active medium, e.g. using photonic devices [3, 4, 6]. Photonic devices can in many cases be viewed as the introduction of surface modulations to an existing system, purposely designed to exploit field-enhancing resonant phenomena such as guided-mode resonances and/or plasmonic effects. Grating structures, designed to phase match incident light with modes supported by an underlying core material, enable wave propagation confined to the regions defined by the core boundaries [9, 10]. Similarly, tuning the plasmonic response of metal nanostructures by tailoring their design, allows for extreme local field enhancement [11].

A complete upconverter-assembly comprising, among others, erbium ions and optimized photonic devices embedded into a suitable host, could be placed on the rear side of a solar cell. The rear-placement ensures that the photonic devices only interact with the infrared light transmitted through the cell, thus not interfering with the intrinsic photon-absorption.

Such an embedded setup is one potential end goal for designing field-enhancing devices, however, considering instead a setup with photonic device placed on top of thin film is also of great interest, e.g. for photonic crystal biosensors [12] and polarization-tuned color filters [13]. For such a configuration, one question is, how to efficiently couple incident light into the film and how to systematically target different field-enhancing mechanisms?

Optics EXPRESS

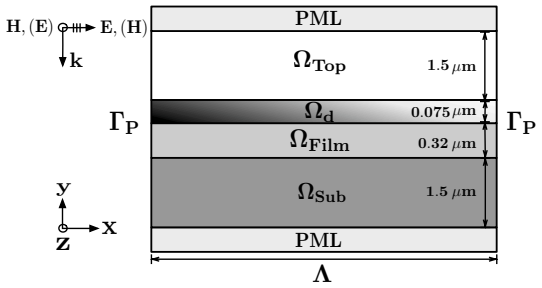

Fig. 1. Model problem. Domain truncation at the top and bottom using perfectly matched layers (PML) [14,15] and periodicity is imposed at Γ_P using Floquet-Bloch conditions [14,15].

This work addresses these questions by utilizing an optimization-based design method and formulating a selection rule for selecting the dominant field-enhancing mechanism, of a periodic array of identical metallic nanostrips place on top of a erbium-doped thin film. The nanostrip design is optimized for electric-field enhancements in the film, targeting enhanced spectral upconversion, when excited by normally incident infrared light. The underlying physical mechanisms responsible for the observed field-enhancements are investigated by optimizing for varying periodicity and interpreting the results using waveguide analysis. The topology optimization method is used as a numerical synthesis tool to design the 2D nanostrip cross section (assuming the strips are extruded infinitely in the out-of-plane direction).

2. The model problem

The 2D model problem considered in this work is shown in Fig. 1. It is comprised of a top domain of air (Ω_{Top}) and an erbium-doped TiO_2 (TiO_2:Er) thin film (Ω_{Film}) deposited onto a SiO_2 substrate (Ω_{Sub}). The system is excited by a time-harmonic plane wave at normal incidence, polarized in either the x- or z-direction (in-plane and out-of-the-plane of Fig. 1, respectively). The electric-field distribution, $\boldsymbol{E}$, in the model is obtained by solving the electric wave equation, for each polarization using the finite element method, assuming linear, isotropic, and non-magnetic materials without any external charges or currents. To enhance the field in Ω_{Film}, in turn increasing the upconversion luminescence, incident light is focused into the film by an optimized distribution of air and Au (i.e., the nanostrips) in the design domain, ($\Omega_d \subset \Omega_{\text{Top}}$), placed on top of the film.

3. The selection rule

Photonic devices, exploiting waveguide excitation, offer field-enhancements spanning large areas but they are generally limited by a narrow spectral band of operation. Plasmonic structures, on the contrary, are typically associated with a much broader operation band and strong local enhancements. Control of these enhancement mechanisms enable devices designed for specific use cases.

The proposed selection rule is based on a map showing the possibility for coupling to guided modes as a function of incident wavelength, λ, and grating period, Λ, such as the one in Fig. 2. This map enables the user, prior to performing the optimization, to determine the field-enhancing mechanism of the optimized design by carefully selecting values of (λ, Λ). The map is calculated from waveguide and phase-matching analysis based on the materials chosen for Ω_{Top}, Ω_{Film}, and Ω_{Sub} as well as the designable material used in Ω_d. The selection rule is therefore not limited to the materials or specific dimensions stated in section 2. The conditions for waveguide excitation is based on using the two extreme material distributions obtainable in Ω_d, which in turn is shown to provide valuable insight about the field-enhancing mechanisms for all investigated material distributions intermediate to the two extrema. In this work, the extrema are: (I) Ω_d full of air

and (II) Ω_d full Au (the height of Ω_d (75 nm) corresponds to roughly 3 times the Au skin depth (25 nm) at $\lambda = 1520$ nm, thus extremum (II) is the electromagnetic equivalent to Ω_{Top} filled Au). It is noted that the analysis depends on the incident angle, ϕ, of the exciting wave (here only normal incidence, $\phi = 0°$, is considered).

The following steps outline the procedure for obtaining the map, for the device shown in Fig. 1, as well as how to select (λ, Λ).

- **(a)** Choose the materials for the substrate, film, top domain and the designable material. A high refractive index, η, of the film relative to the top domain and substrate is a prerequisite for mode confinement in the film, i.e. $\max\{\eta_{Top}, \eta_{Sub}\} < \eta_{Film}$ [16].
- **(b)** Assuming a 2D infinitely wide slab waveguide (independent of Λ), calculate the supported guided modes for a range of λ, by solving the polarization-dependent mode equations for the propagation-constant $\beta_m(\lambda)$ at the m^{th} mode [16]. The mode number, m, describes the mode shape/electric-field distribution in the film, see e.g. [16]. The calculated $\beta_m(\lambda)$ is the x-component of the propagating (guided) waves k-vector. This step has to be performed for both material extrema (I) and (II) and for all considered polarizations, e.g. x- and/or z-polarization.
- **(c)** Supported modes are excited efficiently by an incoming plane wave if phase matching is fulfilled, i.e. if the mismatch between incident the wave vector $\boldsymbol{k}$ and β_m is balanced by a grating structure. Thus, for each $\beta_m(\lambda)$ obtained in step **(b)**, solve the phase-matching condition: $\|\boldsymbol{k}\| \sin(\phi) = \beta_m(\lambda) + 2\pi n \Lambda^{-1}$ for Λ, considering an interval of $n \in \{-N, \ldots, -2, -1, 0, 1, 2, \ldots, N\}$, with N being an integer. The order of diffraction, n, describes the direction/order of the diffracted wave with respect to the grating normal [9]. For $\phi = 0°$, the matching condition reduce to: $\beta_m(\lambda) = -2\pi n \Lambda^{-1}$. This step leads to a value of Λ for each considered $\beta_m(\lambda)$ and n.
- **(d)** Create the lines in the (λ, Λ)-map by plotting the solutions found from step **(c)**, see the black and blue lines in Fig. 2. For each polarization, every m and n: highlight the regions spanned by the lines for extrema (I) and (II). In Fig. 2, these regions are shown in light- and dark-gray between pairs of solid and dashed lines (black and blue).
- **(e)** Use the map to select (λ, Λ)-values to target the desired field-enhancement mechanism: for designs exploiting waveguide excitation select (λ, Λ) within a highlighted region and for pure plasmonic designs select (λ, Λ) outside these regions. As shown in section 5, it is, for the presented case, possible to select (λ, Λ) obtaining a mix of plasmonic and waveguide enhancement.
- **(f)** For the specified (λ, Λ)-values, design the nanostrips using an optimization method of choice.

Figure 2 shows a map of the phase-matching condition for the fist two diffracted orders $n \in \{1, 2\}$ for $\Lambda \in [500\,\text{nm}, 2000\,\text{nm}]$ and $\lambda \in [1400\,\text{nm}, 1600\,\text{nm}]$. In the considered interval of λ, the 320 nm thick film supports only the first waveguide mode, i.e. $m = 1$ (even mode) see e.g. [16]. Black and blue represent x- and z-polarization, respectively. The dashed lines (excluding the red line) indicate phase-matching for extremum (I) and solid lines for extremum (II). These lines, thus, represent the upper and lower bounds for phase-matching when Ω_d consists only of air or Au. The highlighted regions, between pairs of solid and dashed lines, indicates the (λ, Λ)-span where phase-matching is possible for intermediate air and Au distributions in Ω_d. The map is created following steps **(a)**-**(d)** and calculated using numerical methods similar to those reported in [17].

4. The optimization based design problem

The investigated design problem concerns maximization of the upconversion luminescence under infrared irradiation at $\lambda = 1520$ nm, which has been found to be proportional to $\|\boldsymbol{E}\|^3$ [3, 4, 18].

Optics EXPRESS

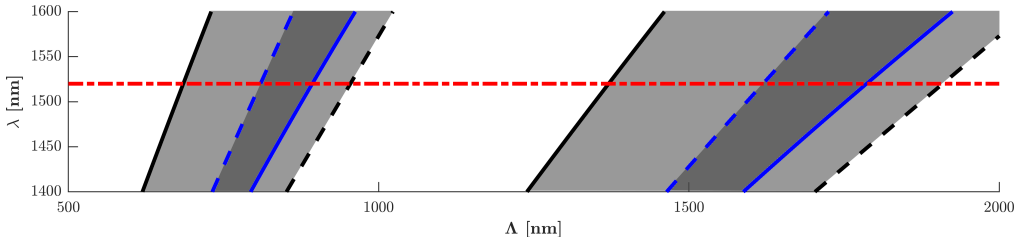

Fig. 2. Black and blue lines show incident wavelength, λ, versus phase-matching period, Λ, for extrema (I) and (II). Lines: black for x-polarization, blue for z-polarization, dashed for extremum (I) and solid for extremum (II). Highlighted regions to the left represent diffractive coupling to the $m = 1$ mode, at $n = 1$ and regions to the right at $n = 2$. The red horizontal line mark the wavelength used in the optimizations, $\lambda = 1520$ nm.

The purpose of step **(f)** in the selection rule thus becomes to identify a nanostrip design/material distribution of air and Au which maximizes $\|\boldsymbol{E}\|^3$ in the film, thereby increasing the spectral upconversion in the erbium. The design of the nanostrips is performed using the topology optimization method.

The goal of topology optimization in its simplest form is to identify a spatial distribution of materials A (in this work air) and B (in this work Au), which maximizes the performance of the system in question expressed through a scalar objective function. The design is represented in a discrete raster format via identical unit cells, pixels (2D) or voxels (3D), each of which is assigned a design variable. The distribution of material is expressed through interpolation in the relevant material properties of A and B using the design variables. In this work, material properties are described by the complex relative electric permittivity entering the wave equation, using the interpolation scheme reported in [6, 7]. For a detailed description of the topology optimization framework the reader is referred to [19, 20] and the references therein.

Using an objective function, Φ, similar to those used in [3, 4, 6, 21] the optimization problem is formulated as

$$\max \quad \Phi_i = \frac{\int_{\Omega_{\text{Film}}} \|\boldsymbol{E}\|_i^3 \mathrm{d}\Omega}{\int_{\Omega_{\text{Film}}} \|\boldsymbol{E}_{\text{b}}\|_i^3 \mathrm{d}\Omega}, \quad \text{subject to:} \quad i = x \vee i = z. \tag{1}$$

Where Φ is dimensionless and evaluates the enhancement of $||\boldsymbol{E}||^3$ in the film, relative to the background field, $\boldsymbol{E}_{\text{b}}$, i.e. without any Au in Ω_{d}. Thus, Φ is a measure of enhanced upconversion luminescence. Equation (1) is solved for either x- or z-polarized light as indicated by the index $i \in \{x, z\}$. The optimization is performed for a range of Λ across the different regions of the map in Fig. 2, to investigate if the optimization conforms to the predicted upper and lower bounds on Λ found in the waveguide and phase-matching analysis, i.e. steps **(b)**-**(d)**. To avoid mapping poor local maxima in the investigation, a multi-start approach is used where for each Λ the optimization is started from multiple randomized initial material distributions. All designs are forced mirror symmetric along a vertical line though the center of Ω_{d}. Material data for Au and SiO_2 are taken from [22] and [23], respectively, while data for TiO_2:Er is obtained experimentally via spectral ellipsometry measurements.

The model and optimization problems are implemented in, and solved using COMSOL Multiphyics® [15]. The optimization is performed using the built-in implementation of the Globally Convergent Method of Moving Asymptotes (GCMMA) [24]. A custom MATLAB® code controls and automates the entire process through the LiveLink™ API. The model is discretized by linear non-uniform triangular elements with a maximum size of $\lambda/\eta_j/40$ for the domains $j \in \{\Omega_{\text{Top}}, \Omega_{\text{Film}}, \Omega_{\text{Sub}}\}$ and 2nm uniform linear quadrilateral elements in Ω_{d}. The PML regions are each 2 μm thick and discretized using a maximum element size of 200 nm.

Optics EXPRESS

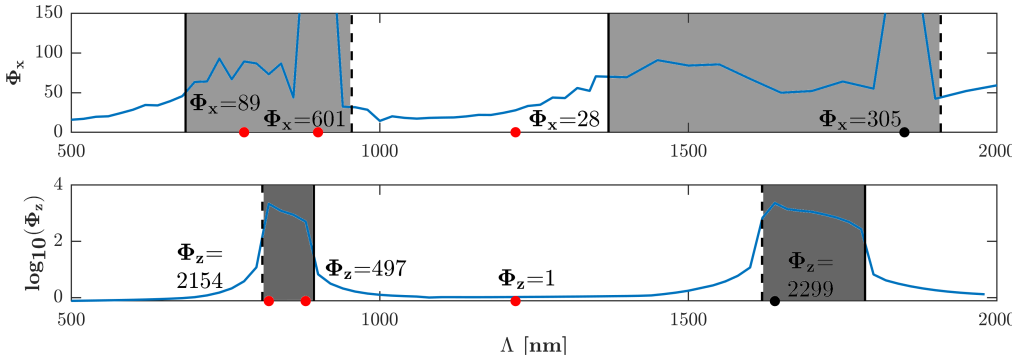

Fig. 3. Objective function value for the best performing designs optimized at $\lambda = 1520\,\text{nm}$. Top: Φ_x. Bottom: Φ_z. The vertical lines indicate the theoretical bounds on Λ for phase-matching to the $m = 1$ mode at $\lambda = 1520\,\text{nm}$ (see Fig. 2). Dots indicate the designs optimized at periods $\Lambda \in [780\,\text{nm}, 900\,\text{nm}, 1220\,\text{nm}, 1850\,\text{nm}]$ (top) and $\Lambda \in [820\,\text{nm}, 880\,\text{mm}, 1220\,\text{nm}, 1640\,\text{nm}]$ (bottom). Designs at periods indicated by red dots are shown in Fig. 4.

5. Results and discussion

The objective function value for the best designs at each period, obtained by the multi-start procedure, are shown in Fig. 3. The vertical lines represent the upper and lower bounds on Λ for phase-matching at $\lambda = 1520\,\text{nm}$ (see Fig. 2). Designs with the highest performance are obtained at periods matching those for guided-mode excitation. This trend is in agreement with the map presented in Fig. 2, and indicates that at these specific periods the optimization exploits field enhancements from excitation of guided modes. Plasmonic resonance is normally associated with highly localized field enhancements, hence when evaluated over large areas as in Eq. 1, the contribution to Φ_i is small relative to the enhancement from a guided mode spanning the entire Ω_{Film}. This explains the drop in Φ_i at intermediate periods where, according to the map in Fig. 2, waveguide coupling is suppressed. A likely explanation as to why the overall picture is less clear for Φ_x, is the possibility for both plasmonic and waveguide field enhancements, which creates additional local maxima for field enhancement compared to Φ_z. (To remove the possibility of a plasmonic response a study optimizing Φ_x using a dielectric material (SiO_2) instead of Au was performed. This study resulted in a curve similar to that of Φ_z in Fig. 3 (SiO_2-curve not shown) supporting the conclusions). Lastly, it is noted that for both polarizations, Φ_i increases drastically near the dashed-vertical lines representing Ω_d filled with air.

Figure 4 shows the field enhancement for selected designs optimized for Φ_x (left) and Φ_z (right) at periods indicated by the red dots in Fig. 3. Designs in the first row are optimized at the intermediate period $\Lambda = 1220\,\text{nm}$ where no waveguide-coupling should be possible. The detailed features of the Φ_x-optimized design create distinct localized enhancements typically attributed to plasmonic resonances. The lack of enhancement from the Φ_z-optimized design, is believed to stem from the assumption of infinite extrusion in the z-direction which makes a plasmonic response impossible when the field excitation is in the z-direction. The second row shows the field enhancement for designs at $\Lambda = 900\,\text{nm}$ (Φ_x) and $\Lambda = 820\,\text{nm}$ (Φ_z) both of which are periods exciting the waveguide mode at $n = 1$ near the air-line (dashed vertical line in Fig. 3). The field characteristics from these designs resemble those normally accredited to mode confinement. Similar behavior is observed for all designs within the bounds for phase-matching (field distributions not show). Finally, designs in the third row are also optimized for periods in the $n = 1$ waveguide region, but offset further from the air-line. The field-enhancement from the Φ_x-design at $\Lambda = 780\,\text{nm}$ carries characteristics of both mode confinement and plasmonic

Optics EXPRESS

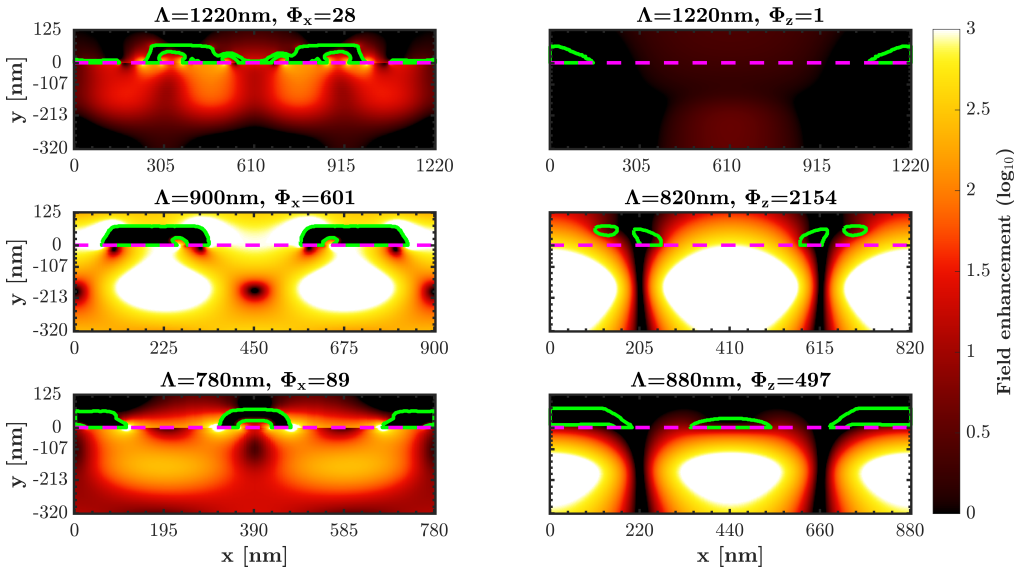

Fig. 4. Field enhancement from designs optimized at periods indicated by the red dots in Fig. 3. Left: optimized for Φ_x showing $\|\boldsymbol{E}\|_x^3/\|\boldsymbol{E}_b\|_x^3$. Right: optimized for Φ_z showing $\|\boldsymbol{E}\|_z^3/\|\boldsymbol{E}_b\|_z^3$. Green lines shows the design contour and magenta lines indicate the interface interface between Ω_d and Ω_{Film}. Ω_{Top} is partly shown and Ω_{Sub} is excluded.

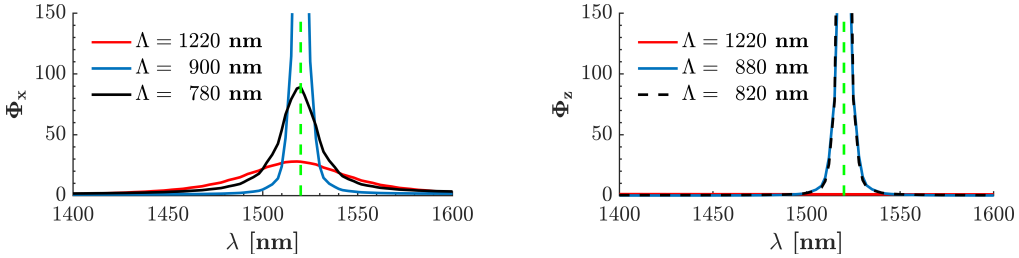

Fig. 5. Performance of the optimized designs shown in Fig.4, evaluated for wavelengths $\lambda \in [1400\,\text{nm}, 1600\,\text{nm}]$. Left: Designs optimized for Φ_x. Right: Designs optimized for Φ_z. The green vertical line indicates the optimization wavelength $\lambda = 1520\,\text{nm}$. Peak values are given in Fig. 3.

enhancement. An explanation for this mixed enhancement-profile is possibly a weaker waveguide coupling, leaving the plasmonic enhancement more pronounced. The Φ_z-design at $\Lambda = 880\,\text{nm}$ shows similar enhancement as the design at $\Lambda = 820\,\text{nm}$, but with a much reduced Φ_z-value, which, again, is assumed due to a less effective waveguide coupling.

To further investigate the contributing field-enhancing mechanisms, the spectral performance, $\Phi_i(\lambda)$, of the six designs is evaluated across a 200 nm wavelength span, the results of which are shown in Fig. 5. The wide peak of the Φ_x-design optimized at $\Lambda = 1220\,\text{nm}$ adds to the notion of plasmon-dominated enhancement outside the waveguide-regions [25]. The narrow and high-valued peaks from the three designs with the periods $\Lambda \in \{900\,\text{nm}, 820\,\text{nm}, 880\,\text{nm}\}$ (Φ_x, Φ_z, Φ_z) indicates diffractive coupling with the designs acting as transmission gratings exciting the guided mode in the film. The mixed enhancement characteristic claimed for the $\Lambda = 780\,\text{nm}$-design (Φ_x) is supported as a wide peak similar to the profile of the $\Lambda = 1220\,\text{nm}$-design ($\Phi_x$) but with 3× the amplitude. Hence a mixture of the waveguide and plasmonic spectral profiles is seen. Similar mixed performance has been observed for other designs optimized for Φ_x, at periods in the waveguide-regions but off-set from the air-line (plots not shown), indicating a subset of

Optics EXPRESS

periods in the waveguide-regions where one can obtain designs exploiting both plasmonic and wave-guiding effects.

It is noted that, the monochromatic optimization at normal incidence does not ensure an enhanced field across a broad wavelength and angular spectrum. The influence of optimizing Au nanostrips for field-enhancement at multiple wavelengths and/or incident angles were investigated in a previous study by the authors [6]. Here, it was found that simultaneously optimizing for multiple wavelength increases the robustness towards changes in incident angle.

The designs in Fig. 4 contain non-realizable features (e.g. floating Au), an aspect which is not addressed in this work as the focus is on evaluating the conditions for waveguide coupling. Several other works have, however, demonstrated methods for including production constraints directly into the topology optimization framework [6, 26, 27].

6. Conclusion

Conditions for phase-matched waveguide-exaction were utilized to formulate a selection rule, which enables the designer to a priori select a desired field-enhancing mechanism obtained when designing metallic nanostrip-arrays on thin-films utilizing optimization-based design tools. The validity of the rule was investigated using topology optimization to design the 2D nanostrip cross section at varying periodicity for enhancing 1520 nm infrared light in an TiO_2:Er thin film, targeting increased spectral upconversion. Optimizing at periods predicted to couple to the guided mode resulted in designs with enhancement profiles attributable to guided modes, i.e. high enhancement factors due to strong confinement of the electric fields but also with a wavelength-sensitive performance. Designs optimized at non-coupling periods resulted in a plasmon-dominated performance with lower overall enhancement but a spectral-enhancement profile less sensitive to changes of the excitation wavelength. Mixed waveguide and plasmonic performance were obtained for designs optimized for x-polarized light, at phase-matched periods off-set from the theoretical air line.

The proposed selection rule is generally applicable to design problems where the goal is to obtain field enhancements in a thin film, using an optimization based design tool to distribute material on top of the film.

Funding

Innovation Fund Denmark under the SunTune project (4106-00002B) and by Villum Fonden through the NATEC (NAnophotonics for Terabit Communications) project.

Acknowledgment

The authors thank Ph.D. Fellows; Søren H. Møller for valuable inputs and Harish Lakhotiya for providing the TiO_2:Er ellipsometry measurements.